Supporting Information

Structural properties determining low K^+ affinity of the selectivity filter in the TWIK1 K^+ channel

Hisao Tsukamoto[1, 2], Masahiro Higashi[3], Hideyoshi Motoki[3], Hiroki Watanabe[4], Christian Ganser[4], Koichi Nakajo[5, 6, #], Yoshihiro Kubo[5, 6], Takayuki Uchihashi[4] and Yuji Furutani[1, 2]*

1 Department of Life and Coordination-Complex Molecular Science, Institute for Molecular Science, 38 Nishigo-Naka, Myodaiji, Okazaki 444-8585, Japan.

2 Department of Structural Molecular Science, SOKENDAI (The Graduate University for Advanced Studies), 38 Nishigo-Naka, Myodaiji, Okazaki 444-8585, Japan.

3 Department of Chemistry, Biology and Marine Science, University of the Ryukyus, Senbaru 1, Nakagami, Nishihara, Okinawa 903-0213, Japan.

4 Department of Physics and Structural Biology Research Center, Graduate School of Science, Nagoya University, Furo-cho, Chikusa-ku, Nagoya 464-8602, Japan.

5 Division of Biophysics and Neurobiology, Department of Molecular Physiology, National Institute for Physiological Sciences, 38 Nishigo-Naka, Myodaiji, Okazaki 444-8585, Japan.

6 Department of Physiological Sciences, SOKENDAI (The Graduate University for Advanced Studies), 38 Nishigo-Naka, Myodaiji, Okazaki 444-8585, Japan.

Current affiliation: Department of Physiology, Division of Life Sciences, Faculty of Medicine, Osaka Medical College

*Correspondence to: furutani@ims.ac.jp

Table of Contents

1. **Supporting Methods**
   Supporting Figure S1
2. **Supporting Figures: Figure S2-7**
3. **Legends for Supporting Movies: Movies S1-11**
4. **References**

1. Supporting Methods

1. 1. *Fluorescence-detected size-exclusion chromatography (FSEC) analysis:* FSEC analysis was conducted according to the procedure of Kawate and Gouaux.[1] Briefly, the cDNA of various two-pore domain K^+ channels (mouse TWIK1, mouse TASK1, human TASK3, human TRAAK, mouse THIK1, and mouse THIK2) were inserted into the EcoRI/XhoI site of the pEGFP-pMT vector, which was designed to produce channels fused with EGFP on the C-terminus. Each construct was transfected into COS-1 cells on a 100 mm diameter plate, as described previously, and harvested after a 48 h incubation. The transfected cells were collected and solubilized with 1% DDM (n-dodecyl-β-D-maltoside) (Dojindo, Kumamoto, Japan), 140 mM KCl, and 20 mM HEPES at pH 7.4, and then centrifuged for 20 min at 100,000 g and 4 °C. The supernatant was directly injected into a Superdex 200 10/300 GL column (GE Healthcare, Pittsburgh, PA) equilibrated with 0.05% DDM, 140 mM KCl, 20 mM HEPES at pH 7. The flow rate was 0.5 mL/min and the EGFP fluorescence was detected using a RF-20A fluorescence detector (Shimadzu, Kyoto, Japan). The excitation wavelength was set to 480 nm, and the emission wavelength was set to 512 nm. COS-1 cells and pMT vectors were gifted by Dr. David Farrens (Oregon Health and Science University).

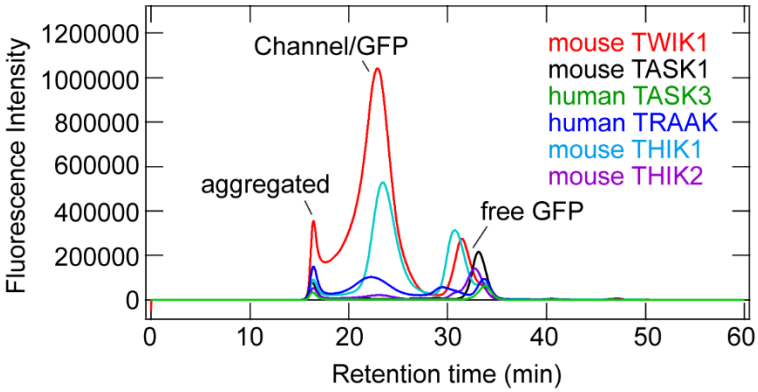

Figure S1. FSEC chromatographs of TWIK1 and other two-pore domain potassium channels.

To assess the expression levels and molecular properties of mouse TWIK1 in our cultured cells, we exploited FSEC analyses for TWIK1 and other two-pore domain potassium channels. Fluorescence chromatographs of C-terminus GFP-tagged two-pore domain channels (mouse TWIK1, mouse TASK1, human TASK3, human TRAAK, mouse THIK1, and mouse THIK2) are shown in Figure S1. TWIK1 showed a high fluorescence intensity peak as well as additional peaks for aggregated and free-GFP species.

1. 2. The sequential binding model constructed for the global fitting analysis:

The sequential binding model involving protein conformation changes can be expressed as follows:

$$\mathrm{n}K^+ + \mathrm{Ch} \overset{K_d1^{(K^+)}}{\longleftrightarrow} K_n^+\mathrm{Ch}$$

and

$$\mathrm{m}K^+ + K_n^+\mathrm{Ch} \overset{K_d2^{(K^+)}}{\longleftrightarrow} K_{n+m}^+\mathrm{Ch}^*,$$

where the dissociation constants can be defined as follows:

$$K_d1^{(K^+)} = \frac{[K^+]^n[\mathrm{Ch}]}{[K_n^+\mathrm{Ch}]}$$

and

$$K_d2^{(K^+)} = \frac{[K^+]^m[K_n^+\mathrm{Ch}]}{[K_{n+m}^+\mathrm{Ch}^*]}.$$

When $[\mathrm{Ch}]_0$ is the net amount of channels in the system,

$$[\mathrm{Ch}]_0 = [\mathrm{Ch}] + [K_n^+\mathrm{Ch}] + [K_{n+m}^+\mathrm{Ch}^*],$$

the fraction of the channel protein in the first K^+ binding step can be expressed as follows:

$$[\mathrm{Ch}] = \frac{K_d1^{(K^+)}[K_n^+\mathrm{Ch}]}{[K^+]^n}$$

$$[K_{n+m}^+\mathrm{Ch}^*] = \frac{[K^+]^m[K_n^+\mathrm{Ch}]}{K_d2^{(K^+)}}$$

$$[\mathrm{Ch}]_0 = \frac{K_d1^{(K^+)}[K_n^+\mathrm{Ch}]}{[K^+]^n} + [K_n^+\mathrm{Ch}] + \frac{[K^+]^m[K_n^+\mathrm{Ch}]}{K_d2^{(K^+)}}$$

$$[\mathrm{Ch}]_0 = \left(1 + \frac{K_d1^{(K^+)}}{[K^+]^n} + \frac{[K^+]^m}{K_d2^{(K^+)}}\right)[K_n^+\mathrm{Ch}].$$

Therefore, the fraction of the channels in the first K^+ binding event can be expressed as follows:

$$f_{K_n^+Ch}^{[K^+]} = \frac{[K_n^+\mathrm{Ch}]}{[\mathrm{Ch}]_0} = \frac{1}{1 + \frac{K_d1^{(K^+)}}{[K^+]^n} + \frac{[K^+]^m}{K_d2^{(K^+)}}}.$$

Similarly, the case for the secondary binding mode can be expressed as follows:

$$[\mathrm{Ch}] = \frac{K_d1^{(K^+)}[K_n^+\mathrm{Ch}]}{[K^+]^n} = \frac{K_d1^{(K^+)}}{[K^+]^n} \times \frac{K_d2^{(K^+)}[K_{n+m}^+\mathrm{Ch}^*]}{[K^+]^m} = \frac{K_d1^{(K^+)}K_d2^{(K^+)}}{[K^+]^{n+m}} \times [K_{n+m}^+\mathrm{Ch}^*].$$

$$[K_n^+\mathrm{Ch}] = \frac{K_d 2^{(K^+)}[K_{n+m}^+\mathrm{Ch}^*]}{[K^+]^m}$$

$$[\mathrm{Ch}]_0 = \frac{K_d 1^{(K^+)} K_d 2^{(K^+)}}{[K^+]^{n+m}} \times [K_{n+m}^+\mathrm{Ch}^*] + \frac{K_d 2^{(K^+)}[K_{n+m}^+\mathrm{Ch}^*]}{[K^+]^m} + [K_{n+m}^+\mathrm{Ch}^*]$$

$$[\mathrm{Ch}]_0 = \left(1 + \frac{K_d 1^{(K^+)} K_d 2^{(K^+)}}{[K^+]^{n+m}} + \frac{K_d 2^{(K^+)}}{[K^+]^m}\right)[K_{n+m}^+\mathrm{Ch}^*]$$

$$f_{K_{n+m}^+Ch^*}^{[K^+]} = \frac{[K_{n+m}^+\mathrm{Ch}^*]}{[\mathrm{Ch}]_0} = \frac{1}{1 + \frac{K_d 1^{(K^+)} K_d 2^{(K^+)}}{[K^+]^{n+m}} + \frac{K_d 2^{(K^+)}}{[K^+]^m}}.$$

1. 3. The equation used for fitting the difference absorbance spectra

The absorbance of the sample when [K$^+$] = x is as follows:

$$\mathrm{Abs(x)} = Abs_{Ch} \times f_{Ch}^x + Abs_{K_n^+Ch} \times f_{K_n^+Ch}^x + Abs_{K_{n+m}^+Ch^*} \times f_{K_{n+m}^+Ch^*}^x,$$

where f is the fraction, and Abs is the absorbance of the different species present (free channel (and/or Na$^+$-bound), first K$^+$ binding mode, second K$^+$ binding mode). Because the summation of all fractions becomes 1, we can express the fraction of the free channel (and/or Na$^+$-bound) (f_{Ch}^x) as a function of the fraction of the channel first K$^+$ binding mode ($f_{K_n^+Ch}^x$), and the second binding mode becomes ($f_{K_{n+m}^+Ch^*}^x$)

$f_{Ch}^x = 1 - f_{K_n^+Ch}^x - f_{K_{n+m}^+Ch^*}^x$.

Therefore,

$$Abs(x) = Abs_{Ch} \times \left(1 - f_{K_n^+Ch}^x - f_{K_{n+m}^+Ch^*}^x\right) + Abs_{K_n^+Ch} \times f_{K_n^+Ch}^x + Abs_{K_{n+m}^+Ch^*} \times f_{K_{n+m}^+Ch^*}^x.$$

Rearranging the equation, we can obtain the following:

$$Abs(x) = Abs_{Ch} + \Delta Abs_{K_n^+Ch-Ch} \times f_{K_n^+Ch}^x + \Delta Abs_{K_{n+m}^+Ch^*-Ch} \times f_{K_{n+m}^+Ch^*}^x,$$

where Δabs is the difference in absorbance between the two species.

The difference in absorbance when one changes the K$^+$ concentration from an initial to a final value becomes

$$\Delta Abs = Abs(x) - Abs(x_0)$$

$$= \Delta Abs_{K_n^+Ch-Ch} \times \left(f_{K_n^+Ch}^x - f_{K_n^+Ch}^{x_0}\right) + \Delta Abs_{K_{n+m}^+Ch^*-Ch} \times \left(f_{K_{n+m}^+Ch^*}^x - f_{K_{n+m}^+Ch^*}^{x_0}\right).$$

In our experiments, the initial concentration of K$^+$ was 0. Therefore, $f_{K_n^+Ch}^{x_0} = f_{K_{n+m}^+Ch^*}^{x_0} = 0$.

Thus, the absorbance difference can be calculated by the following equation:

Equation 1:

$$\Delta Abs = \Delta Abs_{K_n^+ Ch-Ch} \times f^x_{K_n^+ Ch} + \Delta Abs_{K_{n+m}^+ Ch^*-Ch} \times f^x_{K_{n+m}^+ Ch^*}$$

$$= \Delta Abs_{K_n^+ Ch-Ch} \times \frac{1}{1 + \frac{K_d 1^{(K^+)}}{x^n} + \frac{x^m}{K_d 2^{(K^+)}}} + \Delta Abs_{K_{n+m}^+ Ch^*-Ch} \times \frac{1}{1 + \frac{K_d 1^{(K^+)} K_d 2^{(K^+)}}{x^{n+m}} + \frac{K_d 2^{(K^+)}}{x^m}}$$

2. Supporting Figures

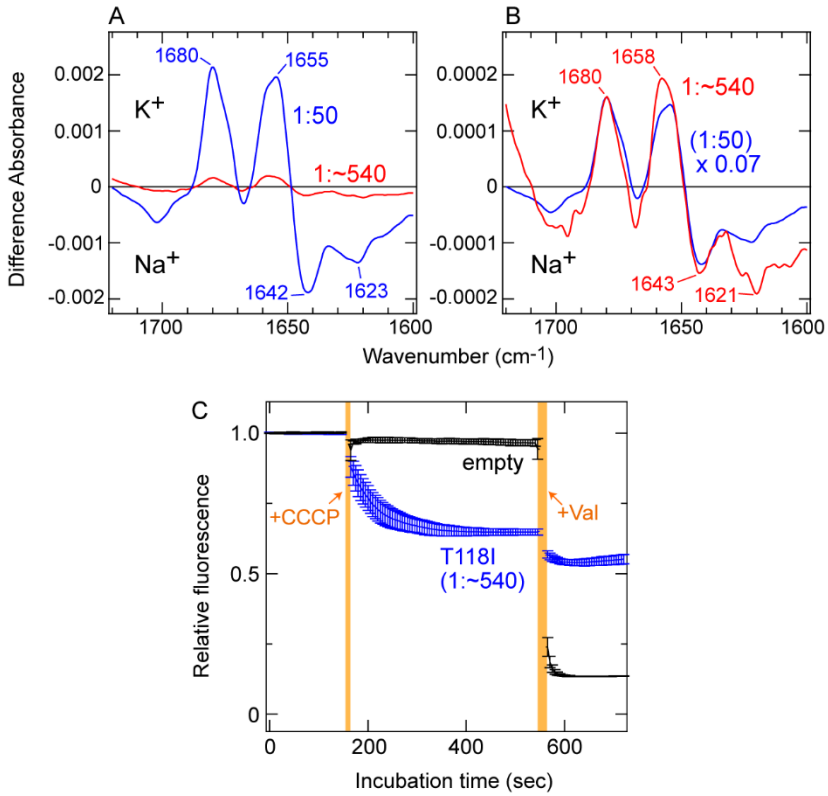

Figure S2. TWIK1 proteoliposomes applicable to both the flux assay and ion-exchange-induced difference spectroscopy experiments

Proteoliposomes containing the TWIK1 T118I mutant (protein/lipid molar ratio = 1 : 540) were prepared and applied to ATR-FTIR measurements and the flux assay. *A*, Difference spectra of the TWIK1 T118I mutant at the protein/lipid molar ratio of 1 : 50 (red) and 1 : 540 (blue). As expected, the signal intensity was significantly reduced as the protein/lipid ratio increased. *B*, When the signal intensity decreased, only the major bands are observed at the protein/lipid molar ratio of 1 : 540 (blue). For comparison, the difference spectrum at the protein/lipid molar ratio of 1 : 50 is also shown (red) after normalization of intensity at 1680 cm^{-1}. *C*, Flux assay using proteoliposomes containing the TWIK1 T118I mutant at the protein/lipid molar ratio of 1 : 540 showed CCCP-dependent fluorescence changes (blue), as shown in Figure 1E. After the addition of valinomycin, differences were observed between the fluorescence levels of empty vesicles (black) and vesicles containing the TWIK1 T118I mutant. This was probably due to difference in property of the liposomes caused by insertion of the channel proteins.

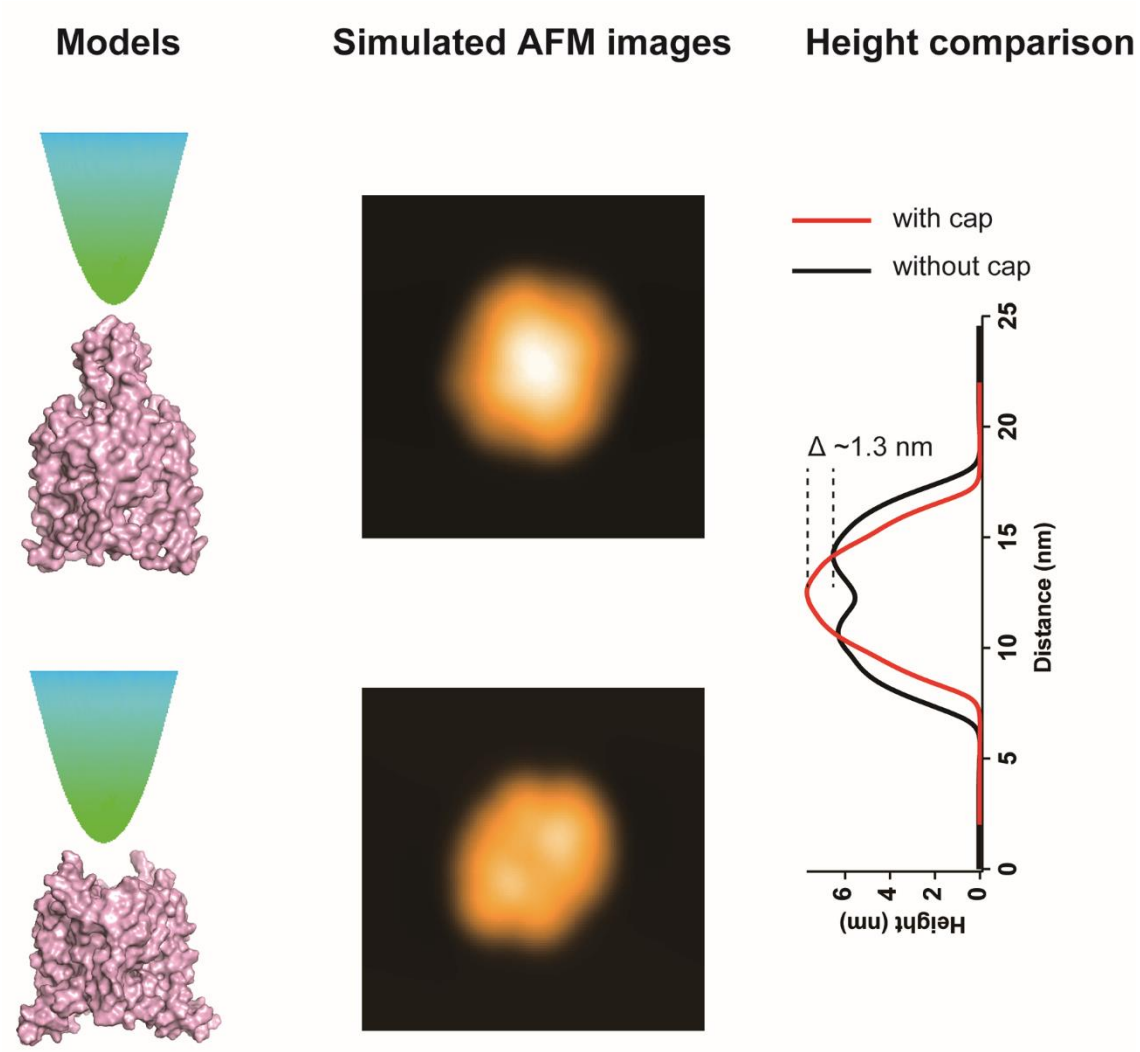

Figure S3. Simulated AFM images and height comparison of TWIK1 channels with and without the extracellular "cap"

The simulated AFM images were calculated by employing a simple hard sphere model using a conical tip (a tip radius of 0.5 nm and a conical half angle of 15°) and the crystal structure of TWIK1. For the WT TWIK1, the crystal structure (PDB code: 3UKM) was used. The model structure TWIK1 without the cap was equilibrated using a molecular dynamics simulation after deletion of residues Pro47 to Asn101. The simulated AFM images were further processed with a low-pass filter with a cut-off wavelength of 2 nm because the spatial resolution of HS-AFM was generally limited to 2 nm^2. The height difference between the channel with and the one without the cap was approximately 1.3 nm, which was in good agreement with the experimentally found difference between the WT (or T118I) and Δcap.

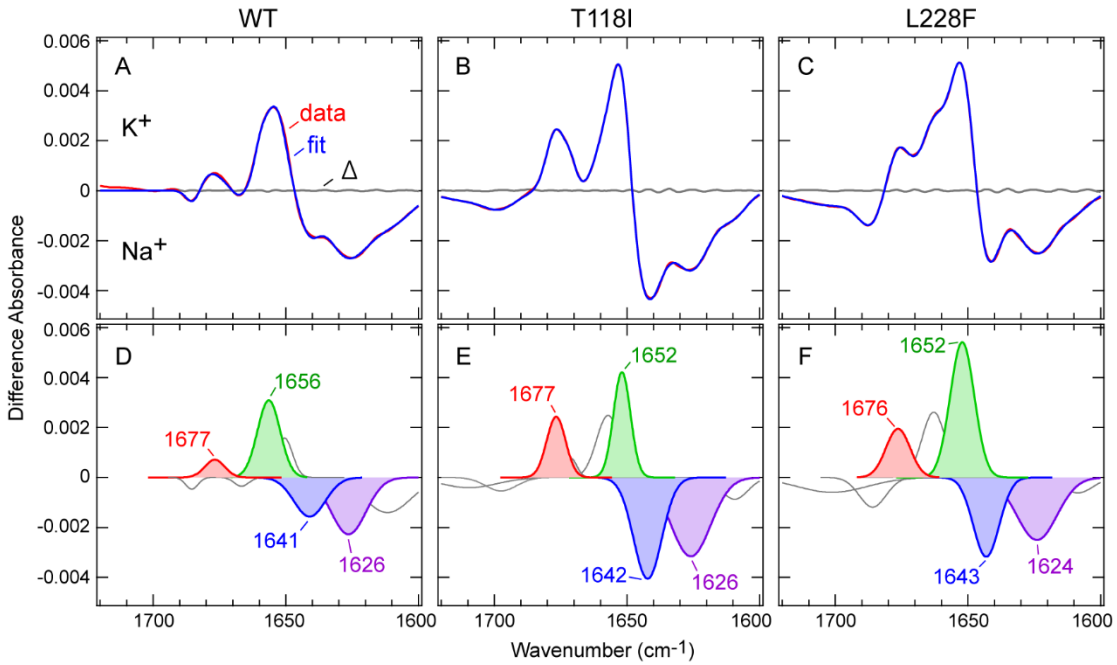

Figure S4. The ion-exchange-induced difference IR spectra of WT TWIK1 and the T118I and L228 mutants obtained in D_2O buffer conditions

A-C, Spectral changes in the amide-I region (red) of TWIK1: WT (*A*), T118I mutant (*B*), L228F mutant (*C*) in D_2O are fitted with seven to eight Gaussian peaks (blue). Residuals are shown in grey. *D-F,* Gaussian peaks of TWIK1 used in the fittings (panels *A-C*): WT (*D*), T118I mutant (*E*), and L228F mutant (*F*). The major peaks are highlighted for clarity.

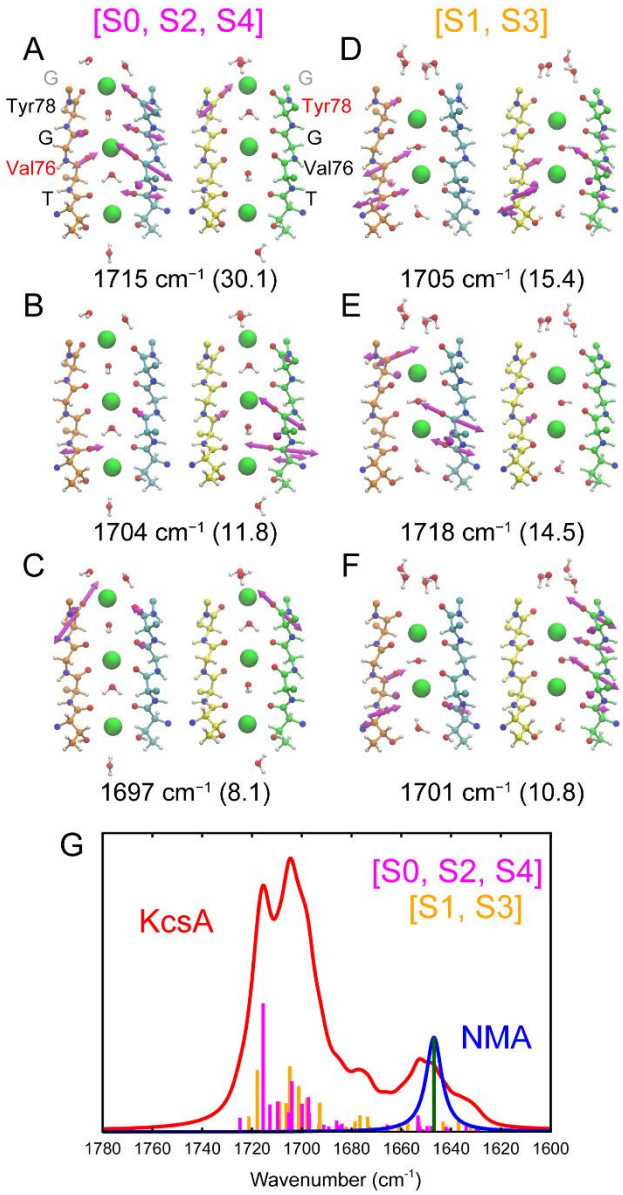

Figure S5. The normal mode analysis of the KcsA selectivity filter using QM/MM calculations

The vibrational vectors for the normal modes of the three highest IR intensities for [S0, S2, S4] (A–C) and [S1, S3] (E–F) configurations. The P1 and P2 domains of the selectivity filter are shown on the left and right sides, respectively. The frequency for each normal mode is shown in the bottom with its intensity in parenthesis. G, The calculated IR absorption spectra of the KcsA selectivity filter (red) and *N*-methyl acetamide (NMA) (blue). The IR intensities of all carbonyl vibrational modes in the KcsA selectivity filter and NMA are shown as bar graphs (magenta: KcsA [S0, S2, S4], orange: KcsA [S1, S3], and green: NMA).

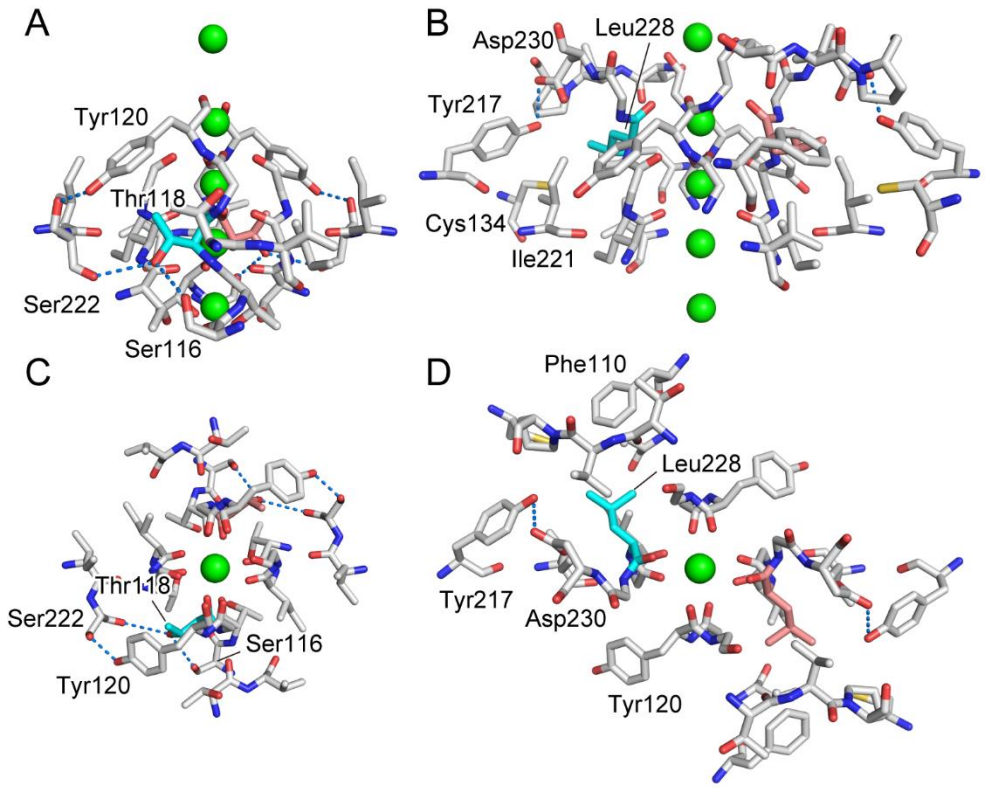

Figure S6. Amino acid residues around Thr118 and Leu228 in the crystal structure of TWIK1

Illustrations of the X-ray crystal structure of TWIK1 around the Thr118 and Leu228 residues. The illustrations in this figure are based on the crystal structure of TWIK1 (PDB ID: 3UKM). A, The selectivity filter region around Thr118 (colored cyan and magenta) viewed from the lateral side. Possible hydrogen-bonding interactions are depicted by blue dotted lines. The hydroxyl group of Thr118 probably forms hydrogen bonds with the hydroxyl groups of Ser116 and Ser222. The carbonyl group of Ser222 is hydrogen-bonded to the phenol group of Tyr120. B, The selectivity filter region around Leu228 (colored cyan and magenta) viewed from the lateral side. Leu228 is surrounded by hydrophobic amino acid residues; therefore, there are no specific interactions with Leu228. C and D, The top views of A and B, respectively.

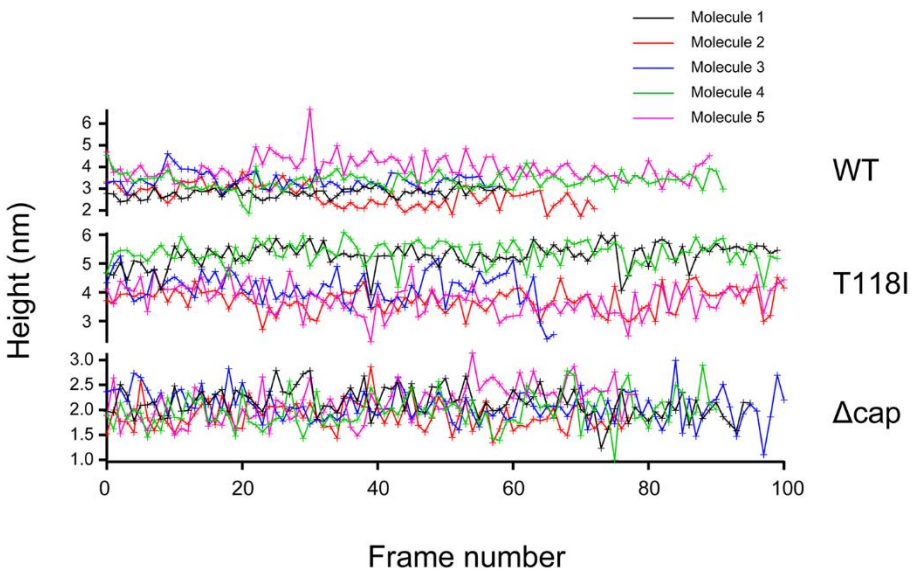

Figure S7. Fluctuations of the height of a single TWIK1 molecule analyzed by HS-AFM (top: WT, middle: T118I, and bottom: Δcap)

Fluctuations of the height of a single molecule are traced for five molecules in each sample. The frame rates are 0.2–0.5 frame/s.

1. 4. Legends for the Supporting Movies

Movie S1. MD simulation of TWIK1 with three K^+ ions in the [S0, S2, S4] configuration
Movie S2. MD simulation of TWIK1 with two K^+ ions in the [S1, S3] configuration
Movie S3. MD simulation of KcsA with three K^+ ions in the [S0, S2, S4] configuration
Movie S4. MD simulation of KcsA with two K^+ ions in the [S1, S3] configuration
Movie S5. Comparison of the MD simulation of TWIK1 with that of KcsA with three K^+ ions in the [S0, S2, S4] configuration viewed around Thr118
Movie S6. Comparison of the MD simulation of TWIK1 with that of KcsA with three K^+ ions in the [S0, S2, S4] configuration viewed around Leu228
Movie S7. Comparison of the MD simulation of TWIK1 with that of KcsA with two K^+ ions in the [S1, S3] configuration viewed around Thr118
Movie S8. Comparison of the MD simulation of TWIK1 with that of KcsA with two K^+ ions in the [S1, S3] configuration viewed around Leu228
Movies S1–S8 were constructed from 300 snapshots retrieved at 1 ps intervals and played at the speed of 10 frames/s for 30 s in total.

Movie S9. HS-AFM observation of a single molecule of TWIK1 (WT) channel in KCl or NaCl
Movie S10. HS-AFM observation of a single molecule of TWIK1 (T118I) channel in KCl or NaCl
Movie S11. HS-AFM observation of a single molecule of TWIK1 (Δcap) channel in KCl or NaCl
Movies S9–S11 were constructed from 30 snapshots retrieved in 0.2–0.5 s intervals and played at the speed of 10 frames/s and for 3 s in total.

1. 5. References

1. Kawate, T.; Gouaux, E., Fluorescence-detection size-exclusion chromatography for precrystallization screening of integral membrane proteins. *Structure* **2006,** *14* (4), 673-681.
2. Uchihashi, T.; Iino, R.; Ando, T.; Noji, H., High-speed atomic force microscopy reveals rotary catalysis of rotorless F(1)-ATPase. *Science* **2011,** *333* (6043), 755-8.